Supplementary Information

Sex-dependent effects of neonatal hyperoxia on prefrontal cortex development

Xingrao Ke, Wei Yu, Carl F Schreck, Joseph M Varberg, Melissa A Gener, Daniel A Louiselle, Sheng Xia, Sherry M Mabry, Heather L Menden, Venkatesh Sampath, Robert H Lane, Kaela M Varberg

Content	Page #
Materials and Methods	2
Supplementary Figure 1. Neonatal hyperoxia (HOX) alters prefrontal cortex cellular composition in a sex-specific manner.	6
Supplementary Figure 2: Neonatal hyperoxia (HOX) suppresses myelination related genes in OPCs in a sex-specific manner.	7
Supplementary Figure 3: Neonatal hyperoxia (HOX) alters promoter accessibility of Ttr and long Mbp transcripts in the prefrontal cortex in a sex-specific manner.	8
Supplementary Figure 4. Neonatal hyperoxia (HOX) alters promoter accessibility of Ptchd1 and Kdm3a in a sex-specific manner.	9
Supplementary Figure 5: Neonatal hyperoxia (HOX) reconfigures diseases related regulatory networks in OPCs in a sex-specific manner.	10
Supplementary Figure 6. Neonatal hyperoxia (HOX) reconfigures myelination-associated regulatory networks in OPCs in a sex-specific manner.	11
Supplementary Figure 7. Neonatal hyperoxia (HOX) selectively increases KDM3A expression in female mouse and human prefrontal cortex.	12
References Cited in Supplement	13

Other Supplementary Files Related to the Submission but not included in the PDF:

Supplementary Tables 1-7 (Excel files)

Materials and Methods

Animals

Timed-pregnant wild type (WT) C57BL/6 mice were purchased from Charles River (Stilwell, KS). Pups and their dams were housed in a hyperoxia chamber from postnatal day (P) 1 to P14. The chamber was continuously flushed with oxygen and maintained at 85% O_2 using a Pro-ox oxygen controller (BioSpherix, Parish, NY). Control mice were housed under identical conditions without hyperoxia exposure. To minimize maternal effects, two dams were rotated daily between the hyperoxia and normoxia groups. At P14, pups were anesthetized with an intraperitoneal injection of pentobarbital (100 mg/kg) and euthanized by exsanguination. Brains were harvested for immunohistochemical analyses or prefrontal cortex tissue was dissected and snap frozen in liquid nitrogen for molecular analyses. For snRNA-seq and snATAC-seq experiments, three female and three male mice per group, each from a different litter, were analyzed. For validation studies, four female and four male mice per group from four distinct litters were analyzed.

snRNA-seq and snATAC-seq

Frozen prefrontal cortex tissue samples from normoxia and hyperoxia-exposed mice (n = 3 per sex per group, from three different litters) were used for snRNA-seq and snATAC-seq analyses. Nuclei were isolated from 40-50 mg of flash-frozen mouse brain tissue using the Chromium Nuclei Isolation Kit with RNase Inhibitor (PN-1000494, 10x Genomics, Pleasanton, CA, USA) according to the manufacturer's protocol, with a final nucleus resuspension volume of 100 µL. Nuclei were stained with AOPI (CS2-0106-5ML, Revvity, Waltham, USA) and quantified using the Cellometer Auto 2000 (Revvity). For each sample, a total of 16,100 nuclei were loaded into one lane of a Chromium Next GEM Chip J (PN-1000234, 10x Genomics) to achieve an estimated recovery of 10,000 nuclei per sample. Single-nucleus partitioning was performed using a Chromium Controller (10x Genomics). snATAC-seq and GEX libraries were prepared using the Chromium Next GEM Single Nucleus Multiome ATAC + Gene Expression Reagent Bundle (PN-1000283, 10x Genomics) following the manufacturer's protocol, and libraries were sequenced on a NovaSeq 6000 Xp (Illumina, San Diego, CA, USA).

Sequencing data analysis

Sequenced RNA and ATAC reads were initially processed by the 10x Genomics Cell Ranger-arc v2.0.0 (1, 2) which includes fastq creation, read alignment, gene counting, peak counting, and cell calling. All samples were mapped to the Cell Ranger-arc mm10 (2020-A-2.0.0) reference genome provided by 10X Genomics. The resulting cell-by-gene and cell-by-peak count matrices were then processed using the following steps in Seurat v5 (3, 4) and Signac v1(5). Cells were filtered out based on the number RNA/ATAC read count, the number of RNA/ATAC features detected, the nucleosome signal, the transcription start site enrichment factor, and the mitochondrial percentage. We applied a quality control filter and kept cells within three median absolute deviations. Next, a common set of ATAC peaks were created for each of the 12 datasets, a joint RNA/ATAC assay for each dataset was created using the common peaks, and then all resulting datasets were merged into a single dataset. After QC filters, our dataset consisted of 39,185 cells (9,796 per group). RNA counts were then normalized using SCTransform, linear dimensionality reduction was performed on RNA via PCA and on ATAC via SVD, and non-linear dimensionality reduction was performed on the joint RNA/ATAC data via the weighted nearest-neighbor (WNN) method (5). Cell types were assigned via label transfer using the mouse brain atlas provided by the Allen Institute (6). We further filtered this dataset down to an equal number of cells per mouse and selected only cells classified as isocortex. After this and previous QC filters, our dataset consisted of 27,723 nuclei (6,930 per group). Corresponding to 13 different classes, 48 subclasses, and 121 cell

supertypes in increasing specificity in the Allen mouse brain cell atlas (Supplementary Table 1: Allen taxonomy table) (6). Because we are primarily interested in oligodendrocyte cells, we defined "cell type" to correspond to the fine-grained supertype for cells within Cluster "10 OPC-oligodendrocyte (Oligo)" and to subclass for all other cells, resulting in a total of 50 cell types discovered in our dataset. In the main text (Fig. 1B-F, Table 1), we renumber the classes and present data for the 12 classes with sufficient cell numbers for analysis. To analyze resulting RNA data, we utilized the differential expression capability in Seurat (3) and to analyze the ATAC data, we utilized the coverage plot visualization in Signac (5).

Ingenuity Pathway Analysis

Differentially expressed genes between groups were considered significant at $P < 0.05$, as determined by an unpaired-samples *t*-test. Bioinformatics analyses were then performed using the ingenuity pathway analysis software (version 150276282; Ingenuity Systems, Qiagen China Co., Ltd.), focusing on canonical pathways, diseases and functions. For these analyses, a threshold of adjusted *P*-value <0.05 was applied, and a Z-score of ± 2 was used to indicate significant activation or inhibition.

Integrated regulatory network analysis (IReNA)

IReNA (7) was used to integrate the RNA and ATAC data to construct regulatory transcription factor networks. The data was processed in four main steps: (Step 1) The data was split into 4 groups including control males (ConM), control females (ConF), hyperoxia-exposed males (HOXM), and hyperoxia-exposed females (HOXF). RNA data was processed for each group to identify potential regulatory relationships (transcription factor-target pairs) using GENIE3 (8). (Step 2) ATAC data was used to refine the potential regulatory relationships obtained from Step 1 by finding footprints via HiNT (9), finding motifs via FIMO (10), linking peaks to transcription factors via Signac (9). IReNA was then used to construct transcription factor-footprint-motif-gene relationships. (Step 3) A modularized regulatory network was created using pseudotime trajectories via monocle3 (11). Pseudotime trajectories were separated into modules and enriched intramodular relationships were identified with IReNA. (Step 4). Finally, a simplified inter-modular network was constructed by identifying modules with significant, shared regulatory activity.

In vitro studies

Mouse brain OPCs were isolated from P5 control mouse pups, cultured and differentiated following the protocol for the acquisition and maturation of oligodendrocyte cells from neonatal rodent brains (12). For hyperoxia experiments, mouse OPCs were cultured in a molecular incubator camber (MIC-101, Embrient Inc, San Diego, CA) containing 85% O_2 and 5% CO_2 for 24 h and 48 h, respectively. Cells were then harvested for RNA isolation or fixed with 4% paraformaldehyde in phosphate buffered saline at room temperature for 10 minutes for immunocytochemical analyses. For OPC differentiation assays, cells were exposed to hyperoxic conditions (85% O_2) for 48 h. Following hyperoxia exposure, cells were cultured in OPC proliferation medium lacking epidermal growth factor for 2 days and subsequently maintained in oligodendrocyte cell differentiation medium for 5 days under normoxic conditions (13). Each experiment was repeated at least three times.

For human OPCs derivation, human iPSCs (AICS-0090-391, Corielle Institute for Medical Research, Camden, NJ, USA) were maintained in mTeSR™ Plus medium (100-0276, STEMCELL Technologies, Cambridge, MA) and differentiated into neural stem cells by culturing in human pluripotent stem cell (hPSC) Neural Induction Medium (5931, ScienCell, Carlsbad, CA) for 7 days, as previously described (13). iPSC-derived neural stem cells were subsequently differentiated into oligodendrocyte cell states following Gibco protocols (Thermo Fisher Scientific). Briefly, neural stem cells were seeded onto poly-ornithine– and laminin-coated

culture plates and maintained in neural stem cell expansion medium (5941, ScienCell) for 2 days. Cells were then cultured in oligodendrocyte cell differentiation medium consisting of Neurobasal medium supplemented with 2% B-27 serum-free supplement, 2 mM GlutaMAX, and 30 ng/mL triiodothyronine (T3) for 3–4 weeks. The derived OPCs were then exposed to hyperoxic conditions (60% O_2) for 24 h or 48 h in a controlled incubator (50145502, Thermo Fisher Scientific, Waltham, MA), respectively for RNA isolation or immunocytochemical analysis as described above. Each experiment was repeated at least three times.

RNA Isolation and Real Time RT-qPCR

Total RNA extraction was performed using *Quick*-RNA Microprep Kit (R1051, Zymo Research, Irvine, CA, USA). Complementary DNA was synthesized by High-Capacity cDNA Reverse Transcription Kit (4374966, Thermo Fisher Scientific, Waltham, MA, USA). Mouse mRNA levels of *Mbp, Plp1, Olig2,* and *Kdm3a* were normalized to *Gapdh* and calculated by the Pfaffl Method (14). Human mRNA levels of the same genes were normalized to 18S rRNA, which served as the internal control. Primers for the genes mentioned above were purchased from Integrated DNA Technologies (Coralville, Iowa, USA) and are listed in Supplementary Table 7. Four to six per sex/group from distinct litters were used for the experiments. Each experiment was repeated at least three times.

RNAscope™ in situ hybridization, Immunofluorescence and Immunocytochemistry

RNAscope™ in situ hybridization was performed to detect *Mbp* (451491-C2, ACDBio, Newark, CA, USA) and *Ptchd1* (489651-C3, ACDBio) mRNA in oligodendrocyte cells identified by the marker *Sox10* (43593, ACDBio) in mouse brain. The assay utilized the RNAscope™ Multiplex Fluorescent Reagent Kit v2 with TSA Vivid dyes (323270, ACDBio), following the manufacturer's instructions. Fourteen de-identified autopsy samples of human neonatal prefrontal cortex tissue (n=3 per group for females and n=4 per group for males) were obtained from the Department of Pathology at Children's Mercy Hospital, Kansas City. The cause of death (COD) for these samples was listed in Supplementary Table 6. Samples from patients who died with BPD were classified as the hyperoxia group, while samples from patients without BPD served as controls. Mouse and human brains were fixed in 4% paraformaldehyde, embedded in paraffin, and sectioned coronally at 4 µm. Immunohistochemistry was performed to assess the protein levels of MBP (NB600-717SS, Novus, Centennial, CO, USA), PLP1 (NB100-1608, Novus), OLIG2 (AF2418, Novus), KDM3A (sc-376608, Santa Cruz Biotechnology, Dallas, TX, USA), and KI67 (9129S, Cell Signaling, Danvers, MA, USA) in P14 mouse and neonatal human brains, following the formalin-fixed paraffin-embedded tissue immunofluorescence protocol (biotechne.com). Double staining was performed to assess KDM3A and KI67 expression in oligodendrocytes using KDM3A/SOX10 (NB21-1091SS, Novus) and KI67/SOX10 antibody pairs. Immunocytochemistry was conducted to evaluate MBP, PLP1, and phospho-H3 (Ser10) expression in mouse OPCs following hyperoxia exposure compared to normoxia, according to the immunofluorescence and immunocytochemistry protocols provided by Biotechne (biotechne.com).

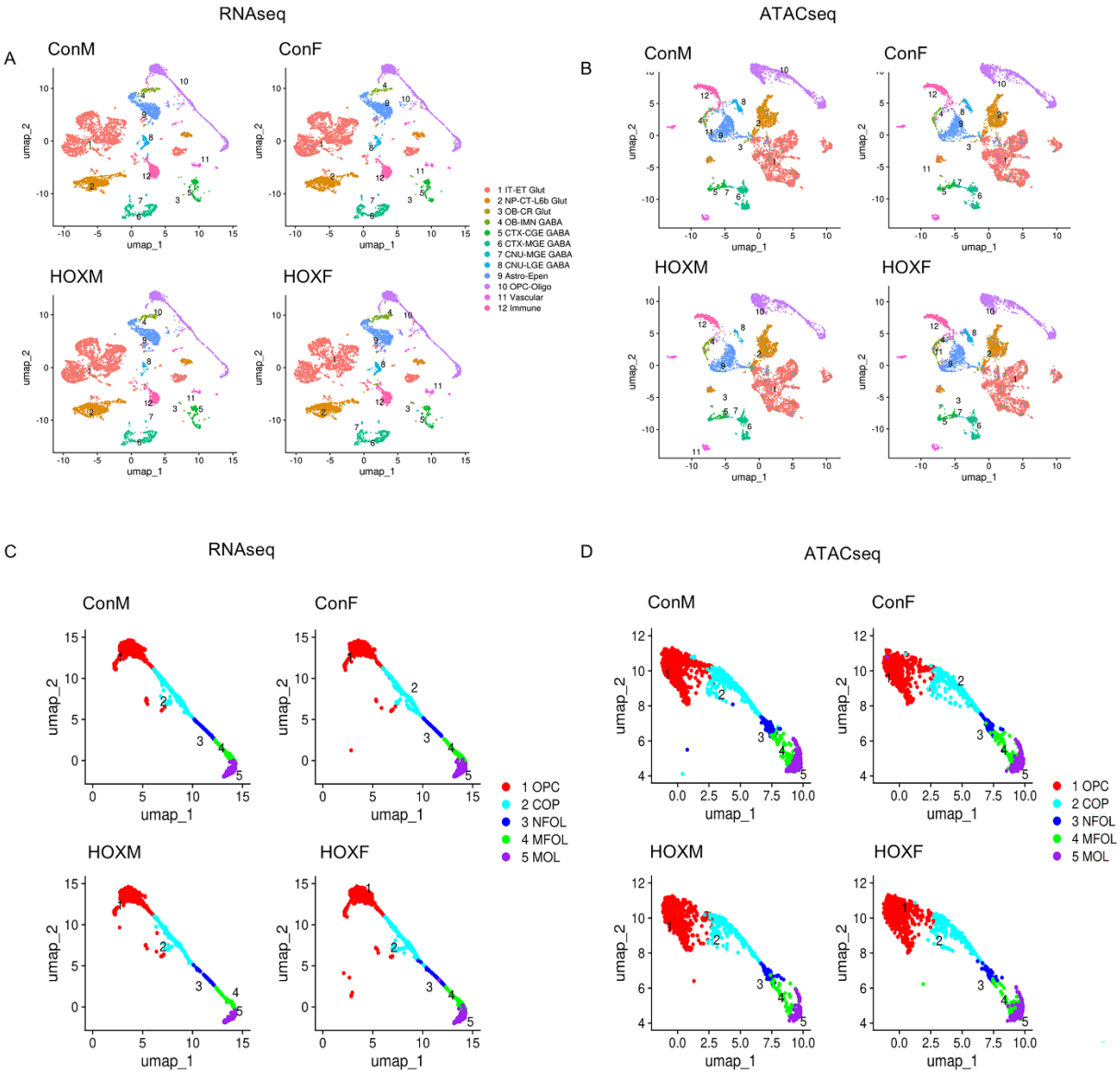
Image capture and quantitation

Images of RNAscope™ in situ hybridization, immunofluorescence and immunocytochemical experiments were captured by Nikon W1 spinning disk confocal microscope (Japan). For quantification, the images of RNAscope™ in situ hybridization and immunofluorescence from mouse and human brains were captured at 20x magnification with 5 µm Z-stacks across 3-10 fields per section. Immunocytochemistry images were acquired at 20x magnification using 3x3 frame tiling per field, with 3-4 fields captured per sample. Imaris® software (v10.2.0, Bitplane, UK) was used to quantify the total areas of MBP and PLP1, as well

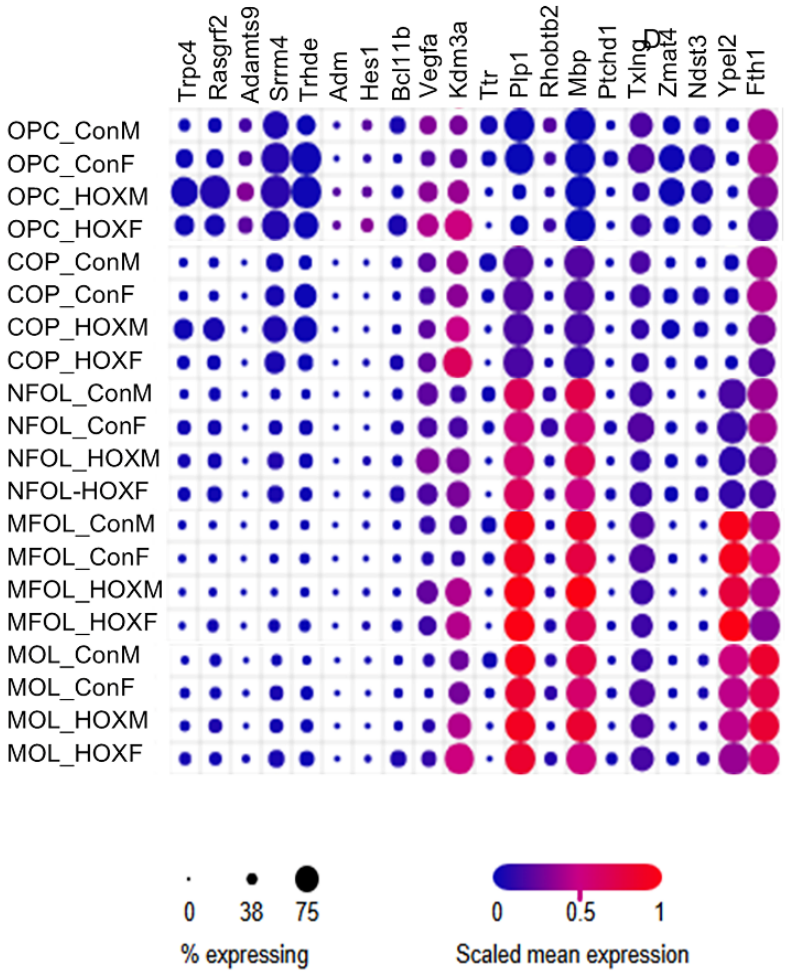
as to determine cell counts for *Ptchd1*$^{+}$/*Sox10*$^{+}$, OLIG2^{+}, KDM3A^{+}/SOX10^{+}, KI67^{+}/SOX10^{+}, and phospho-H3 (Ser10)$^{+}$ populations.

Statistics

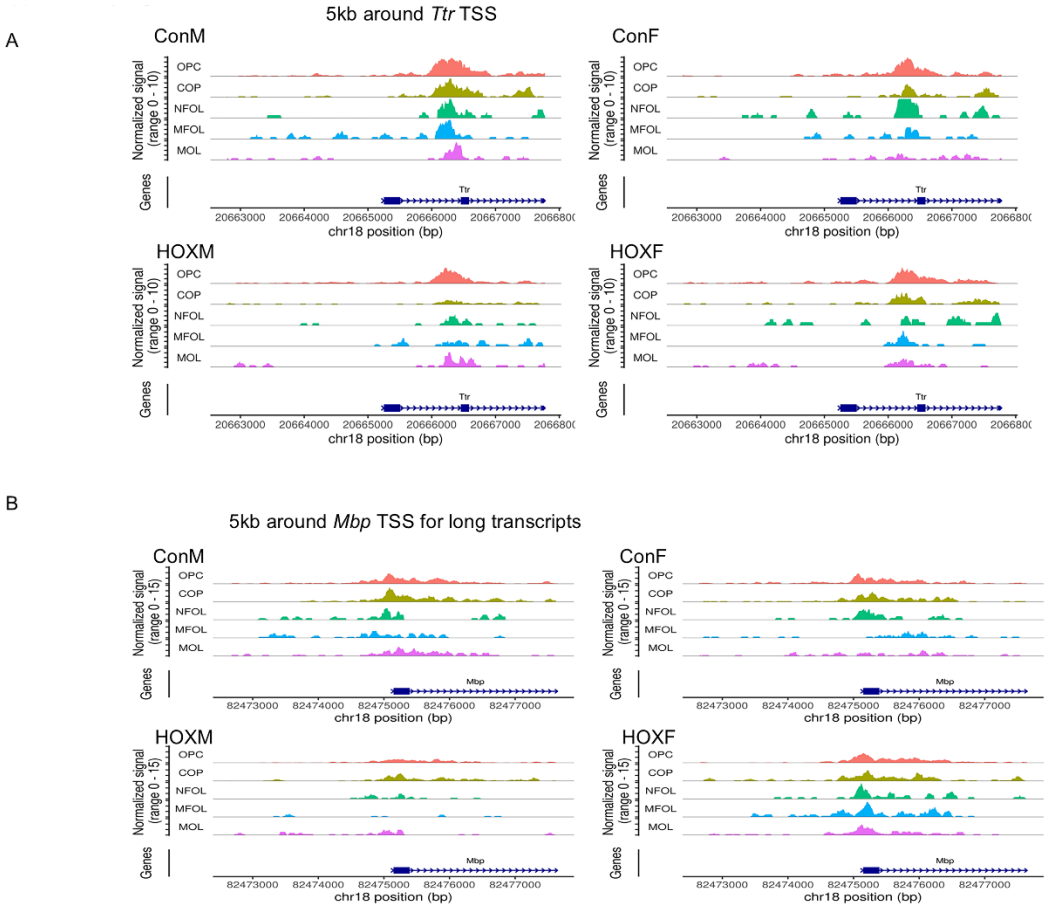
Cell type proportions between two groups were compared by finding the fraction of cells classified as a particular cell type for the three mice in each group and then running a double-sided T-Test to detect p-values. Groups were considered to have significantly different cell type proportions if $p<0.05$. We use Seurat's FindMarkers function when comparing differential expression or peaks between two different groups. This calculated p-values using Wilcoxon rank sum test and adjusted p-values using the Bonferroni correction (15). GraphPad Prism 10 (GraphPad Software, San Diego, CA) was used to perform all analyses for the validation experiments. All data presented are expressed as mean ± standard deviation (SD) and the Mann-Whitney test was used as indicated in figure legends. Statistical significance was set a priori as $p<0.05$.



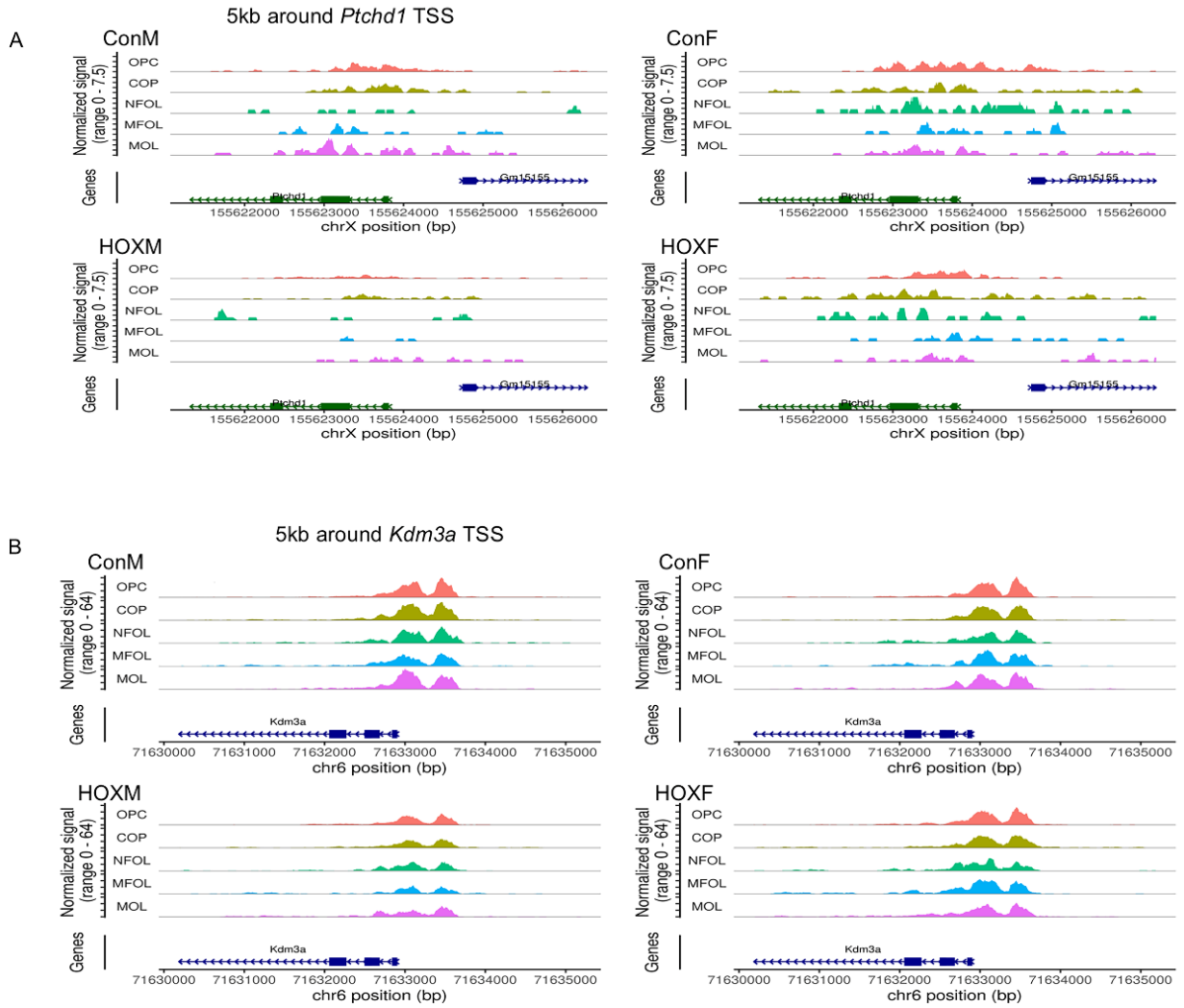
Supplementary Figure. 1: Neonatal hyperoxia (HOX) alters prefrontal cortex cellular composition in a sex-specific manner. Four groups were compared and include: control males (ConM), control females (ConF), hyperoxia-exposed males (HOXM), and hyperoxia-exposed females (HOXF). **(A)** UMAP visualization of prefrontal cortex snRNA-seq data, identifying 12 major cell class. **(B)** UMAP visualization of prefrontal cortex snATAC-seq data, identifying 12 major cell classes. **(C)** UMAP visualization of oligodendrocyte cells from snRNA-seq data, showing five identified supertypes across four groups. OPC = oligodendrocyte (OL) precursor cells, COP = committed OPCs, NFOL= newly formed OLs, MFOL = myelin-forming OLs, MOL = mature OLs. **(D)** UMAP visualization of oligodendrocyte cells from snATAC-seq data, showing five identified supertypes across four groups. *N*=3 mice/sex/group.



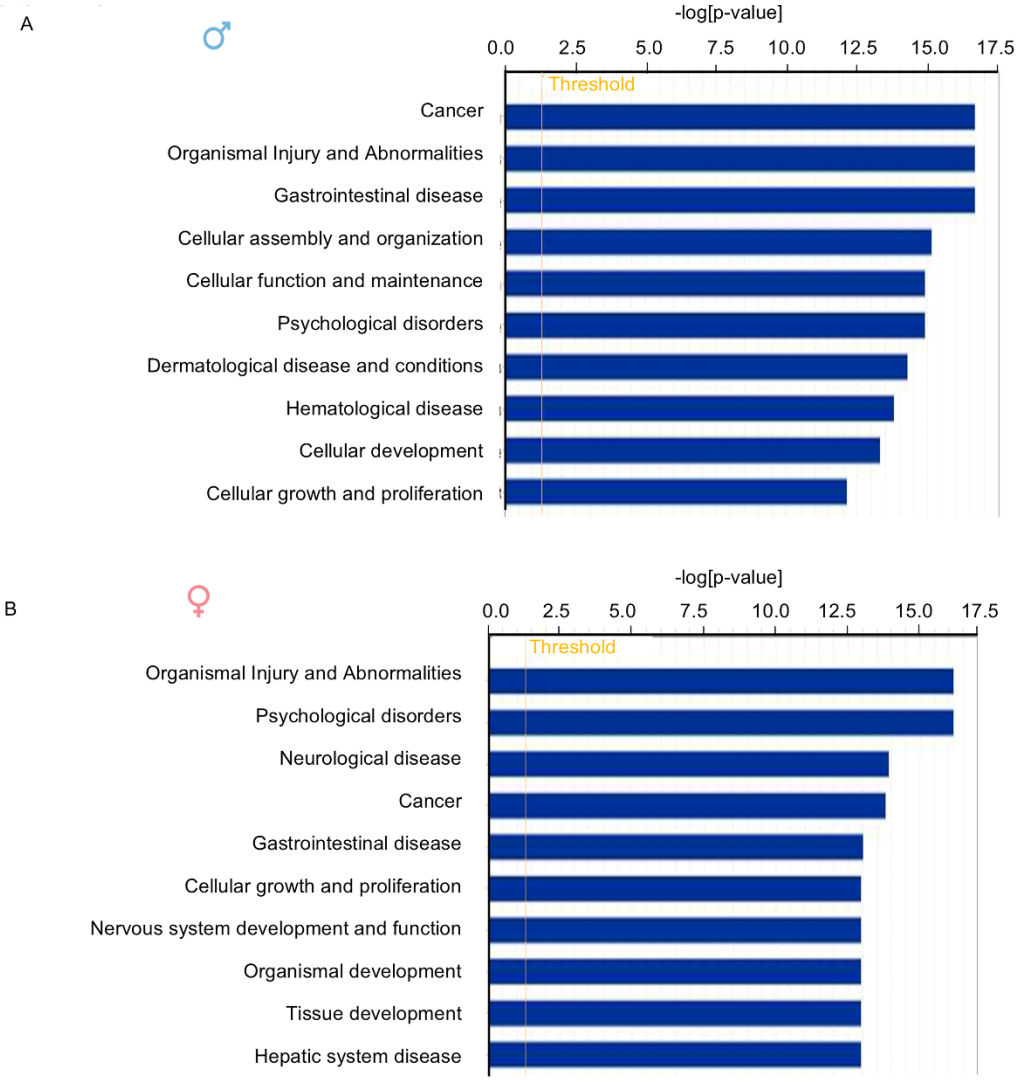
Supplementary Figure 2: **Neonatal hyperoxia (HOX) suppresses myelination related genes in OPCs in a sex-specific manner.** Dot plots of the top 10 upregulated and downregulated genes across five oligodendrocyte cell supertypes in the PFC. OPC = oligodendrocyte (OL) precursor cells, COP = committed OPCs, NFOL= newly formed OLs, MFOL = myelin-forming OLs, MOL = mature OLs. ConM = control males, ConF = control females, HOXM = HOX males, HOXF = HOX females. The size of each dot reflects the percentage of cells expressing the gene, and the color gradient indicates expression level, with blue representing the lowest expression and red representing the highest. N = 3 mice per sex per group from three independent litters.



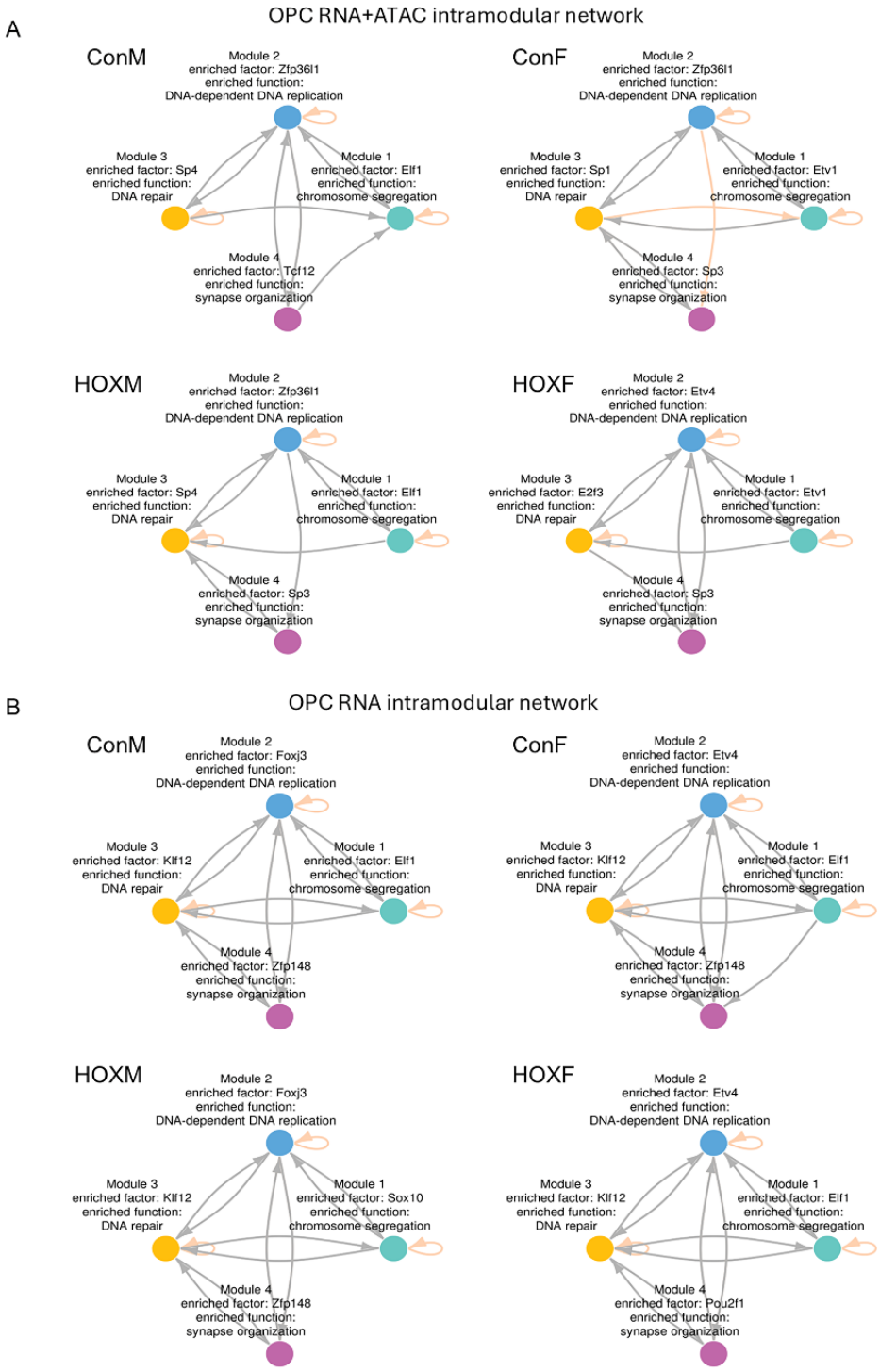
Supplementary Figure 3: **Neonatal hyperoxia (HOX) alters promoter accessibility of *Ttr* and long *Mbp* transcripts in the prefrontal cortex in a sex-specific manner.** Four groups were compared and include: control males (ConM), control females (ConF), hyperoxia-exposed males (HOXM), and hyperoxia-exposed females (HOXF). OPC = oligodendrocyte (OL) precursor cells, COP = committed OPCs, NFOL= newly formed OLs, MFOL = myelin-forming OLs, MOL = mature OLs. **(A)** Differential chromatin accessibility plots from snATAC-seq data for the *Ttr* promoter region across five oligodendrocyte cell supertypes in the mouse prefrontal cortex. **(B)** Differential chromatin accessibility plots from snATAC-seq data for the promoter region of long *Mbp* transcripts across five oligodendrocyte cell supertypes in the mouse prefrontal cortex. *N*=3 mice/sex/group.



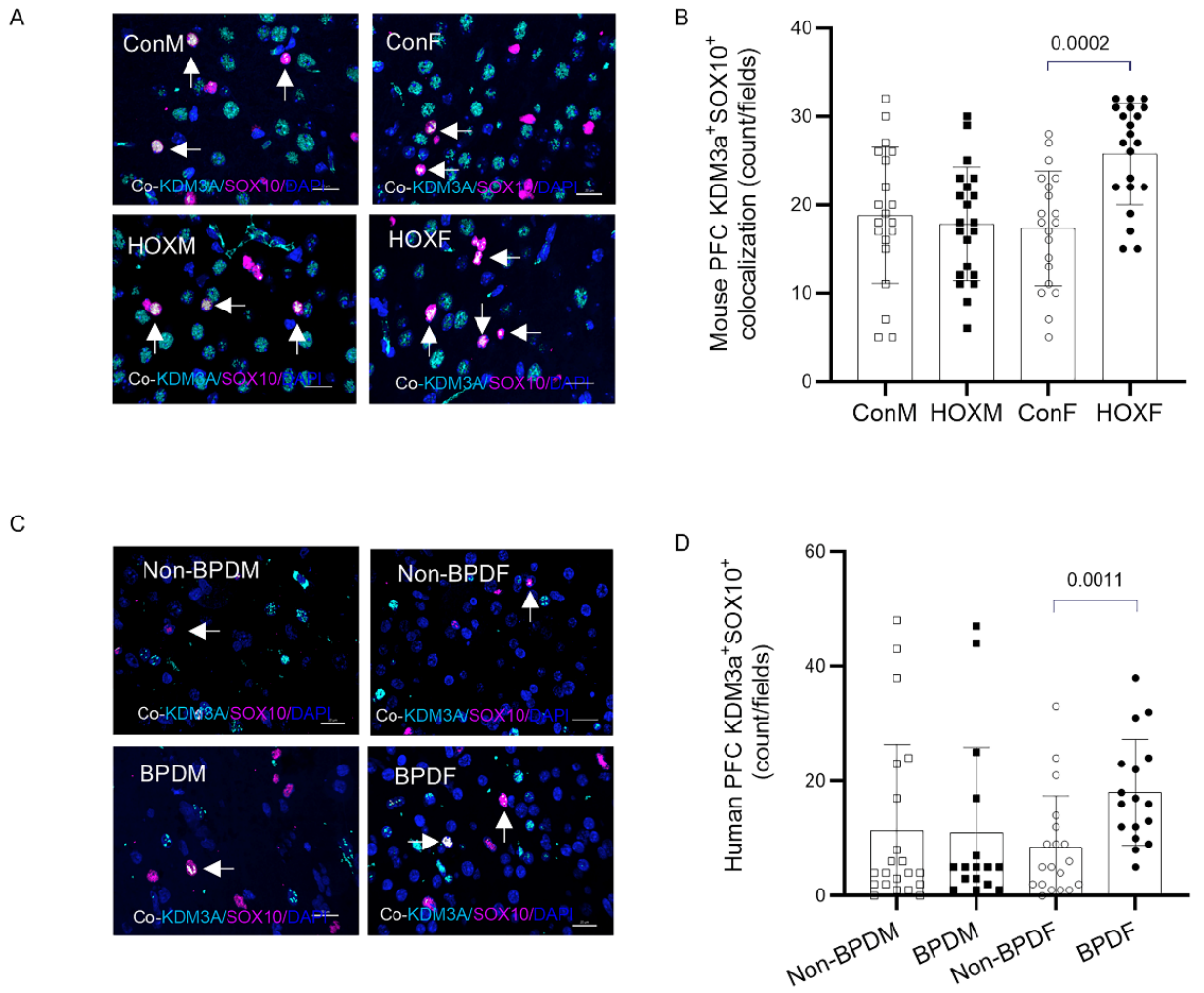
Supplementary Figure 4: **Neonatal hyperoxia (HOX) alters promoter accessibility of *Ptchd1* and *Kdm3a* in the prefrontal cortex in a sex-specific manner.** Four groups were compared and include: control males (ConM), control females (ConF), hyperoxia-exposed males (HOXM), and hyperoxia-exposed females (HOXF). OPC = oligodendrocyte (OL) precursor cells, COP = committed OPCs, NFOL= newly formed OLs, MFOL = myelin-forming OLs, MOL = mature OLs. **(A)** Differential chromatin accessibility plots from snATAC-seq data for the *Ptchd1* promoter region across five oligodendrocyte cell supertypes in the mouse prefrontal cortex. **(B)** Differential chromatin accessibility plots from snATAC-seq data for the *Kdm3a* promoter region across five oligodendrocyte cell supertypes in the mouse prefrontal cortex. *N*=3 mice/sex/group.



Supplementary Figure 5: **Neonatal hyperoxia (HOX) reconfigures diseases related regulatory networks in OPCs in a sex-specific manner. (A)** Top 10 biological functions or diseases predicted by Ingenuity Pathway Analysis in OPCs in males. (**B)** Top 10 biological functions or diseases predicted by Ingenuity Pathway Analysis in OPCs in females. *N*=3 mice/sex/group.



Supplementary Figure 6: **Neonatal hyperoxia (HOX) reconfigures myelination-associated regulatory networks in OPCs in a sex-specific manner.** Four groups were compared and include: control males (ConM), control females (ConF), hyperoxia-exposed males (HOXM), and hyperoxia-exposed females (HOXF). **(A)** Regulatory network pathways derived from snRNA-seq and snATAC-seq data in OPCs. **(B)** Regulatory network pathways derived from snRNA-seq data in OPCs. Orange lines indicate predicted activation while gray lines indicate predicted repression. Orange circular arrows indicate predicted positive self-regulation. *N*=3 mice/sex/group.



Supplementary Figure 7: **Neonatal hyperoxia (HOX) selectively increases KDM3A expression in the female mouse and human prefrontal cortex.** Four groups were compared and include: control males (ConM), control females (ConF), hyperoxia-exposed males (HOXM), and hyperoxia-exposed females (HOXF). **(A)** Immunofluorescence double staining for KDM3A (cyan) and SOX10 (magenta) in the mouse prefrontal cortex, DAPI (blue) for nucleus counterstaining. Colocalization of KDM3A and SOX10 results in a white signal, indicating overlapping expression. White arrows indicate KDM3A$^+$ SOX10$^+$ cells. Scale bar = 20μm. **(B)** Quantitative analysis of KDM3A$^+$ SOX10$^+$ cell numbers in the mouse prefrontal cortex. *N*=4 mice/sex/group. A total of 20-21 fields per group were captured and analyzed, representing 5-6 fields per brain across four distinct brain sections. Data are presented as mean ± SD. **(C)** Immunofluorescence dual staining for KDM3A (cyan) and SOX10 (magenta) in the human prefrontal cortex, DAPI (blue) for nucleus counterstaining. Colocalization of KDM3A and SOX10 results in a white signal, indicating overlapping expression. White arrows point to KDM3A$^+$ SOX10$^+$ cells. Non-BPDM indicates non-BPD male controls, *N*=4; BPDM indicates BPD males, *N*=4; Non-BPDF indicates non-BPD female controls, *N*=3; BPDF indicates BPD females, *N*=3. Scale bar = 20μm. **(D)** Quantitative analysis of KDM3A$^+$ SOX10$^+$ cell numbers in the human prefrontal cortex. Five to six image fields were captured per brain section, resulting in a total of 17-20 fields analyzed per group. The Mann-Whitney test was used to determine the statistical significance between the groups. *P*-values ≤ 0.05 were considered statistically significant.

References Cited in Supplementary Document

1. Satpathy AT, Granja JM, Yost KE, Qi Y, Meschi F, McDermott GP, et al. Massively parallel single-cell chromatin landscapes of human immune cell development and intratumoral T cell exhaustion. *Nat Biotechnol.* 2019;37(8):925–36.
2. Zheng GX, Terry JM, Belgrader P, Ryvkin P, Bent ZW, Wilson R, et al. Massively parallel digital transcriptional profiling of single cells. *Nat Commun.* 2017;8:14049.
3. Hao Y, Hao S, Andersen-Nissen E, Mauck WM, 3rd, Zheng S, Butler A, et al. Integrated analysis of multimodal single-cell data. *Cell.* 2021;184(13):3573–87 e29.
4. Hao Y, Stuart T, Kowalski MH, Choudhary S, Hoffman P, Hartman A, et al. Dictionary learning for integrative, multimodal and scalable single-cell analysis. *Nat Biotechnol.* 2024;42(2):293–304.
5. Stuart T, Srivastava A, Madad S, Lareau CA, and Satija R. Single-cell chromatin state analysis with Signac. *Nat Methods.* 2021;18(11):1333–41.
6. Yao Z, van Velthoven CTJ, Kunst M, Zhang M, McMillen D, Lee C, et al. A high-resolution transcriptomic and spatial atlas of cell types in the whole mouse brain. *Nature.* 2023;624(7991):317–32.
7. Jiang J, Lyu P, Li J, Huang S, Tao J, Blackshaw S, et al. IReNA: Integrated regulatory network analysis of single-cell transcriptomes and chromatin accessibility profiles. *iScience.* 2022;25(11):105359.
8. Huynh-Thu VA, Irrthum A, Wehenkel L, and Geurts P. Inferring regulatory networks from expression data using tree-based methods. *PLoS One.* 2010;5(9).
9. Wang S, Lee S, Chu C, Jain D, Kerpedjiev P, Nelson GM, et al. HiNT: a computational method for detecting copy number variations and translocations from Hi-C data. *Genome Biol.* 2020;21(1):73.
10. Grant CE, Bailey TL, and Noble WS. FIMO: scanning for occurrences of a given motif. *Bioinformatics.* 2011;27(7):1017–8.
11. Cao J, Spielmann M, Qiu X, Huang X, Ibrahim DM, Hill AJ, et al. The single-cell transcriptional landscape of mammalian organogenesis. *Nature.* 2019;566(7745):496–502.
12. Kim H, Kim BJ, Koh S, Cho HJ, Jin X, Kim BG, et al. Protocol for the acquisition and maturation of oligodendrocytes from neonatal rodent brains. *STAR Protoc.* 2024;5(4):103327.
13. Chambers SM, Fasano CA, Papapetrou EP, Tomishima M, Sadelain M, and Studer L. Highly efficient neural conversion of human ES and iPS cells by dual inhibition of SMAD signaling. *Nat Biotechnol.* 2009;27(3):275–80.
14. Pfaffl MW. A new mathematical model for relative quantification in real-time RT-PCR. *Nucleic Acids Res.* 2001;29(9):e45.
15. Etymologia: Bonferroni correction. *Emerg Infect Dis.* 2015;21(2):289.